Journal of
Advances in Environmental Health Research

Summer 2021. Volume 9. Number 3

Research Paper

Photocatalytic Degradation of 2,4-Dichlorophenoxyacetic Acid Using $Fe_2O_3/CeO_2/Ag$ Composite Nanoparticles under Ultraviolet Irradiation

Zohreh Karimipour[1], Reza Jalilzadeh Yengejeh[1*], Azadeh Haghighatzadeh[2], Mohammad Kazem Mohammadi[3], Maryam Mohammadi Rouzbahani[4]

1. Department of Environmental Engineering, Ahvaz Branch, Islamic Azad University, Ahvaz, Iran.
2. Department of Physics, Ahvaz Branch, Islamic Azad University, Ahvaz, Iran.
3. Department of Chemistry, Ahvaz Branch, Islamic Azad University, Ahvaz, Iran.
4. Department of the Environment, Ahvaz Branch, Islamic Azad University, Ahvaz, Iran.

Use your device to scan and read the article online

Citation Karimipour Z, Jalilzadeh Yengejeh R, Haghighatzadeh A, Mohammadi MK, Mohammadi Rouzbahani M. Photocatalytic Degradation of 2,4-Dichlorophenoxyacetic Acid Using $Fe_2O_3/CeO_2/Ag$ Composite Nanoparticles under Ultraviolet Irradiation. Journal of Advances in Environmental Health Research. 2021; 9(3):191-200. http://dx.doi.org/10.32598/JAEHR.9.3.1190

http://dx.doi.org/10.32598/JAEHR.9.3.1190

Article info:
Received: 28 Apr 2020
Accepted: 19 Jun 2020
Publish: 01 Jul 2021

Keywords:
$Fe_2O_3/CeO_2/Ag$,
Photocatalytic performance,
Isotherm models,
4-dichlorophenoxyacetic

ABSTRACT

Background: The herbicide 2,4-dichlorophenoxyacetic acid (2,4-D) is used to control of agricultural pests (water and soil) and is among the most widely distributed pollutants in the environment.

Methods: In this study, $Fe_2O_3/CeO_2/Ag$ composite nanoparticles were synthesized using a simple coprecipitation method. The as-synthesized samples were examined using X-ray diffraction, field emission scanning electron microscopy, and X-ray analysis. The photo catalytic activity of the as-synthesized samples was examined through photo degradation of 2,4-dichlorophenoxyacetic acid (2,4-D) under ultraviolet irradiation. The effects of pH, irradiation time, initial 2,4-D concentration and catalyst dose on the photo catalytic performance of $Fe_2O_3/CeO_2/Ag$ composite nanoparticles were investigated through an optimization process. The photo catalytic reaction kinetic data were analyzed using Langmuir-Hinshelwood model, and the absorption equilibrium was examined by Langmuir and Freundlich isotherm models.

Results: The results suggested the second order reaction kinetics as the best model for 2,4-D photo degradation. Moreover, Langmuir isotherm with a higher R2 was reported as the most suitable model. The photo catalytic activities revealed the highest photo degradation percentage for $Fe_2O_3/CeO_2/Ag$ composite nanoparticles with a degradation order as $Fe_2O_3/CeO_2/Ag$ (75.70%)>Fe_2O_3/CeO_2 (36.28%) >CeO_2 (26.92)>Fe_2O_3 (11.96).

Conclusions: Based on the determination of nanomaterial efficiency, its components and photo catalytic properties, can be used to remove this contaminant and other toxic compounds.

*** Corresponding Author:**
Reza Jalilzadeh Yengejeh, PhD.
Address: *Department of Environmental Engineering, Ahvaz Branch, Islamic Azad University, Ahvaz, Iran.*
Phone: *+98 (912) 4794322*
E-mail: *rahma.reza@gmail.com*

1. Introduction

Due to the increase of agricultural and industrial activities, 2,4-dichlorophenoxyacetic acid (2,4-D) has received attention over the past few decades as a systemic herbicide, which can kill most broadleaf weeds [1, 2]. This acid, as a toxic substance with destructive effects on the human and animal health, can be found in over 1500 herbicide products [3]. With high solubility and a relatively poor biodegradability, 2,4-D results in the contamination of groundwater and soil [4, 5]. Toxic compounds must meet acceptable environmental and health standards before entering the environment [6].

A variety of methods have been utilized to treat 2,4-D from water including absorption [7] biological degradation [8], electrochemical degradation [9] and advanced oxidation processes [10]. Cai et al. reported the degradation of 2,4-D by electro-Fenton and using boron-doped diamond anode [11]. Yang et al. aimed to promote the degradation of 2,4-D with fermentative effluents from hydrogen-producing reactor [12]. Li et al. demonstrated the mechanism and enhanced the degradation pathway of 2,4-D by ore-magnetization Fe-C activated persulfate [13]. Cai et al. described degradation and mechanism of 2,4-D by thermally activated persulfate oxidation [14]. It is well-known that photocatalytic degradation is one of the most effective techniques for wastewater treatment. Numerous studies have been studies the photocatalytic role of nanomaterials in the removal of 2,4-D. In this respect, Li et al. suggested CuO-$Co_3O_4CeO_2$ as a heterogeneous catalyst for efficient degradation of 2,4-D by peroxymonosulfate [15]. Sandeep et al. conducted a comparative study on photocatalytic degradation of 2,4-D using hydrothermal TiO_2 and commercial TiO_2 [16]. Safa et al. studied visible-light photocatalytic degradation of 2,4-D in bath and circulated-mode photoreactors [17]. Tho et al. used a novel reduced graphene oxide/$ZnBi_2O_4$ hybrid photocatalyst for visible light degradation of 2,4-D [18]. In another study, the decomposition of 2,4-D with Mn-doped ZnO/Graphene Nano composite was investigated [19]. Li et al. used $LaFeO_3$ for photocatalytic ozonation of 2,4-D [20]. Zhang et al. used simultaneous H_2 generation method for visible-light photocatalytic degradation of aromatic contaminants [21].

In agricultural industry in Khuzestan, Iran, supply sources are exposed to various pesticides, toxic organic chemical compounds resistant to biodegradation such as chlorine, and phosphorus pesticides. Most pesticides include 2,4-D. In the present study, Fe_2O_3/CeO_2/Ag Composite Nanoparticles (CNPs) were produced and applied for the degradation of 2,4-D. We aimed to: 1) investigate the effects of the operating parameters including pH, irradiation time, initial 2,4-D concentration, and catalyst dose, 2) study the absorption isotherms using Langmuir and Freundlich models, and 3) examine photocatalytic reaction kinetics using Langmuir-Hinshelwood model. The synthesis of Fe_2O_3/CeO_2/Ag CNPs is considered to remove 2,4-D. New compounds and the photocatalytic properties of this compound are assessed for the first time in this study.

2. Materials and Methods

All reagents including cerium (III) nitrate, iron (II) nitrate, ammonium hydroxide, silver nitrate, sodium borohydride, 2,4-D, sodium hydroxide and hydrochloric acid were bought from Merck Company. The Crystallinity was characterized by X-ray diffraction (XRD) using Ultima IV multipurpose system with Cu Kα radiation source (λ=0.15406 nm). The composition of the nanoparticles was investigated using a field emission scanning electron microscopy (ZEISS SIGMA VP-500).

Preparation of samples

Fe_2O_3/CeO_2 CNPs were produced by a two-step co-precipitation method. First 0.01 molar solution (100 mL) of cerium (III) nitrate was added into 100 mL of iron (II) nitrate and taken to pH 11 by addition of ammonium hydroxide. The obtained solution was sealed in a beaker and continuously stirred for 48 h. The resulted precipitate was collected by centrifugation (3000 rpm for 10 min), washed with distilled water, and dried at 90 °C for 8 h and kept in the room temperature. It is should be noted that CeO_2 and FeO_3 nanoparticles were prepared according to the mentioned method by removal of iron (II) nitrate and cerium (III) nitrate precursors, respectively. Silver (Ag) nanoparticles were deposited on the surface of Fe_2O_3/CeO_2 structure to fabricate Fe_2O_3/CeO_2/Ag CNPs. Figure 1 illustrates the synthesis procedure to prepare Fe_2O_3/CeO_2/Ag CNPs. In a typical experiment, 0.2 g of as-synthesized Fe_2O_3/CeO_2 CNPs was dispersed into 150 mL of distilled water using sonication. The obtained product along with 0.01 M aqueous solution (20 mL) of silver nitrate was putted into the ice bath under constant stirring for 30 min. Then, 0.002 M aqueous solution (50 mL) of $NaBH_4$ was added slowly into the solution with a constant stirring for 3 h. Afterwards, the reaction mixture was removed from the ice bath and kept in the room temperature for 12 h.

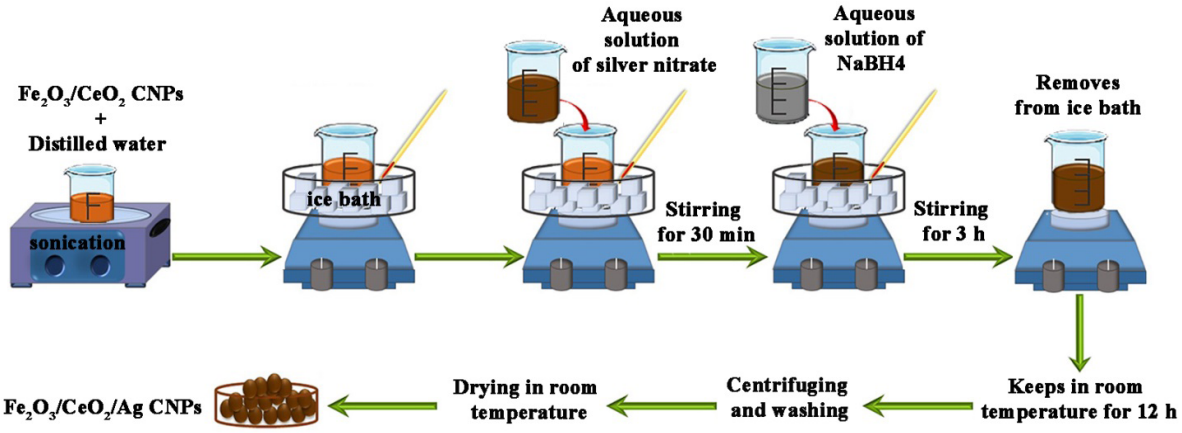

Figure 1. Synthesis steps of Fe_2O_3/CeO_2/Ag CNPs

Photocatalytic activity for 2,4-D degradation

The catalytic efficiency of as-synthesized samples was surveyed for 2,4-D degradation under UV light irradiation. A typical 2,4-D degradation experiment was performed in 250 mL of 2,4-D solution with certain initial concentration, pH and photocatalytic dosage. The used reactor system had two fans to set the temperature at a constant value. After 30 minute in the dark to establish absorption/desorption equilibrium condition, suspensions were irradiated by UV light. 3 mL of solutions was withdrawn regularly after each 30 minutes of irradiation and centrifuged (3000 rpm for 10 minute) to remove catalytic particles. The concentration of 2,4-D in the centrifuged samples was analyzed using a colorimeter (Hach DR/5000), and a characteristic absorption at λmax=202 nm was used to calculate the degradation rate. The absorption capacity in the dark was calculated using Equations 1 and 2 [22-24]:

$$(1)\quad q_e = \frac{(C_0 - C_e)V}{m}$$

where the parameters C0 and Ce are the initial and equilibrium concentrations of 2,4-D in mg/L, respectively; V is the initial solution volume in L, and m is the catalyst amount (g). The degradation percentage of 2,4-D in the presence of UV light was estimated as following [25], where, Ct is the final 2,4-D concentration after absorption equilibrium in mg/L at each irradiated time t.

$$(2)\quad D\,(\%) = \frac{(C_0 - C_t)}{C_0} \times 100$$

3. Results and Discussion

Structural analysis

The phase nature of as-synthesized nanoparticles was examined using XRD. Figure 2 shows the XRD spectra of CeO_2, Fe_2O_3, Fe_2O_3/CeO_2, and Fe_2O_3/CeO_2/Ag samples in 2θ ranging from 20° to 80°. The XRD pattern of CeO_2 sample can be well matched to cubic CeO_2 with space group Fm-3m (01-075-0076). The characteristic peaks of 28.62°, 33.15°, 47.58°, 56.44°, 59.20°, 69.43°, 76.80°, and 79.20° in the pattern were assigned to (111), (200), (220), (311), (222), (400), (331) and (420) planes of cubic CeO_2, respectively. The characteristic peaks of rhombohedral Fe_2O_3 with space group R-3c (01-084-0311) can be also confirmed in the XRD pattern of Fe_2O_3 sample. The reflection peaks at 2θ of 24.2°, 33.10°, 34.50°, 48.62°, 55.10°, 62.32°, and 64.21° can be indexed to (012), (104), (110), (024), (116), (214), and (300) planes of rhombohedral Fe_2O_3, respectively. The XRD pattern of Fe_2O_3/CeO_2 CNPs indicated the presence of cubic CeO_2 structures with revealing (111), (220), (311), (400), and (331) planes (01-075-0076) and rhombohedral Fe_2O_3 structures with revealing (104) and (110) planes (01-084-0311). Four characteristic peaks observed in XRD patterns of Fe_2O_3/CeO_2/Ag CNPs well justified the growth of cubic Ag with space group Fm3m (00-001-1164). The characteristic peaks of 38.14°, 44.32°, 64.47°, and 77.41° in the spectrum corresponded to (111), (200), (220), and (311) planes of cubic Ag structures, respectively.

The results obtained from Field Emission Scanning Electron Microscopy (FESEM) along with the corresponding surface elemental mapping for Fe_2O_3/CeO_2/Ag CNPs are shown in Figure 3. The formation of spherical nanoparticles for Fe_2O_3/CeO_2/Ag CNPs can be seen (Figure 3-A). Fe_2O_3/CeO_2/Ag CNPs exhibited the uniform existence of Fe, Ce, Ag, and O elements in the boxed surface area (Figure 3-B and C).

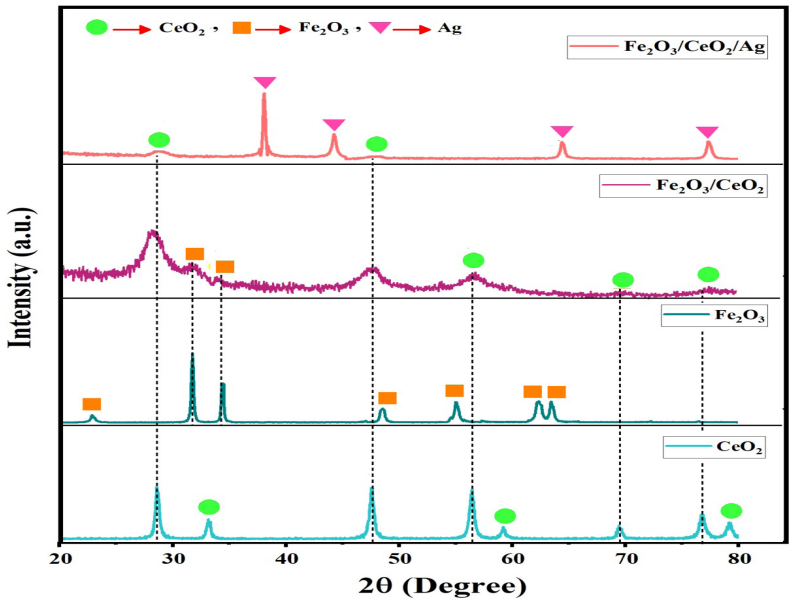

Figure 2. XRD patterns of CeO_2, Fe_2O_3, Fe_2O_3/CeO_2 and Fe_2O_3/CeO_2/Ag CNPs

Absorption equilibrium studies

Isotherm data analysis before irradiation can be useful for estimating the relation between the amount of adsorbed 2,4-D and its equilibrium concentration [26, 27]. The absorption equilibrium data were analyzed using Langmuir and Freundlich models and results for Fe_2O_3/CeO_2/Ag CNPs are presented in Figure 4. Langmuir absorption isotherm can be obtained by the Equations 3 and 4 [28, 29]:

$$(3)\quad \frac{Ce}{q_e}=\frac{1}{q_{max}K_L}+\frac{Ce}{q_{max}}$$

$$(4)\quad R_L=\frac{1}{1+K_LC_0}$$

where qe (mg/g) is the absorption capacity, qmax (Lmg) is the maximum absorption, qmax is the affinity of the binding sites estimated from the intercept of a linear plot of Ce/qe versus Ce, KL (mg/g) is Langmuir constant determined from the slop of Ce/qe versus Ce, RL value shows if the Langmuir isotherm is favorable (0<RL<1) or unfavorable (RL>1). The Freundlich isotherm parameters are defined by the following Equation 5 [30], where KF (mg/g or $(L/mg)^{1/n_F}$) shows the absorption capacity and is estimated from the intercept of the plot of log qe versus log Ce, $1/n_F$ represents the absorption intensity and is obtained from the slop of the line of log qe versus log Ce, and nF value shows if the Freundlich isotherm is favorable ($1<n_F<\phi$) or not (Equations 5) [31]

$$(5)\quad logq_e=logK_F+\frac{1}{n_F}logC_e$$

Absorption equilibrium assessment for Fe_2O_3/CeO_2/Ag CNPs were done on solutions with pH 9, catalyst amount of 0.04 g and with different 2,4-D concentrations (5, 10, 20 and 30 ppm). The results are shown in Figure 4. The numerical values resulted from theoretical fits are presented in Table 1. The RL value was less than 1, indicat-

Table 1. Isotherm parameters for 2,4-D absorption using Fe_2O_3/CeO_2/Ag sample

Sample	Langmuir Model				Freundlich Model			
	qmax (mg/g)	KL (L/mg)	RL	R^2	1/nF(g/mg)	nF(mg/g)	KF (mg/g)	R^2
Fe_2O_3/CeO_2/Ag	22.98	0.22	(0.13) – (0.47)	0.9989	0.071	14.14	17.78	0.9714

Table 2. Kinetic analysis parameters for 2,4-D photodegradation using Fe_2O_3/CeO_2/Ag sample

Sample	Zero-order		First-order		Second-order	
	K0 (mg/L.min)	$R0^2$	K1 (l/min)	$R1^2$	K2 (L/mg.min)	R^2
Fe_2O_3/CeO_2/Ag	0.0028	0.9552	0.0031	0.9579	0.0036	0.9606

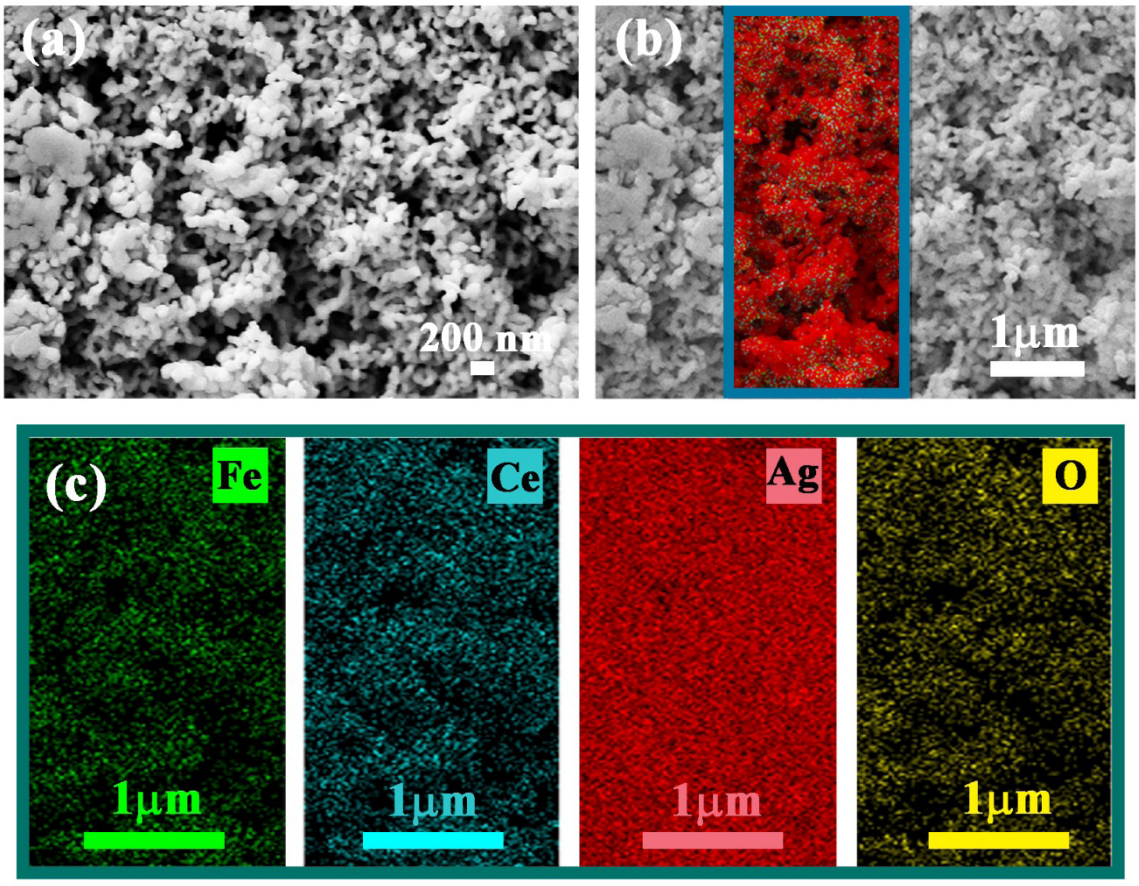

Figure 3. The results obtained from Field Emission Scanning Electron Microscopy (FESEM)

A: FESEM image; B: FESEM map image; and C: The corresponding elemental mappings for $Fe_2O_3/CeO_2/Ag$ sample.

ing a favorable 2,4-D absorption in Langmuir model that occurred on active sites of $Fe_2O_3/CeO_2/Ag$ CNPs with similar affinity. However, the nf was more than 10, indicating an unfavorable absorption of 2,4-D on $Fe_2O_3/CeO_2/Ag$ CNPs under the studied conditions. It can be said that 2,4-D absorption on $Fe_2O_3/CeO_2/Ag$ CNPs was well fitted using both Langmuir and Freundlich models with high correlation coefficients; however, Langmuir isotherm with higher R^2 was more suitable.

Photocatalytic studies

The experiments were performed to investigate the effects of pH, irradiation time, 2,4-D concentration and catalyst dose on the 2,4-D photodegradation. The experiments were carried out in the presence of $Fe_2O_3/CeO_2/Ag$ CNPs. Figure 5-A displays the photodegradation percentage of 2,4-D at different pH values (4, 7, 9 and 11). The results were obtained for solutions with the initial 2,4-D concentration of 10 ppm, nano material amount of 0.02 g, and irradiation time of 120 minutes. The photodegradation rate increased from 0.40% to 41.00% with increasing pH from 4 to 9; however, the photodegradation percentage showed a decrease to 33.30% with further increase of pH value to 11. Therefore, an optimal value equivalent to 9 was considered for pH in the presence of $Fe_2O_3/CeO_2/Ag$ CNPs. The impact of irradiation time on the photodegradation rate with $Fe_2O_3/CeO_2/Ag$ system was studied at specific time intervals of 30 up to 150 minutes. The studies were carried out in the solution with pH=9 and initial 2,4-D concentration of 10 mg/L containing 0.02 g of catalyst and results are plotted in Figure 5-B which suggests an optimal time of 120 min for 2,4-D in the presence of $Fe_2O_3/CeO_2/Ag$ CNPs with a degradation rate equal to 47.36%.

The effect of initial 2,4-D concentration on the photodegradation rate was examined in solutions with pH 9 containing 0.02 g of $Fe_2O_3/CeO_2/Ag$ CNPs. The results for samples with initial 2,4-D concentrations of 5, 10, 20, and 30 ppm after 120 min of UV irradiation are illustrated in Figure 5-C. The increase of initial concentration from 5 to 30 ppm reduced the photodegradation rate from about 55.50% to 22.50%. This suggests an optimal initial 2,4-D concentration of 5 ppm in the presence of

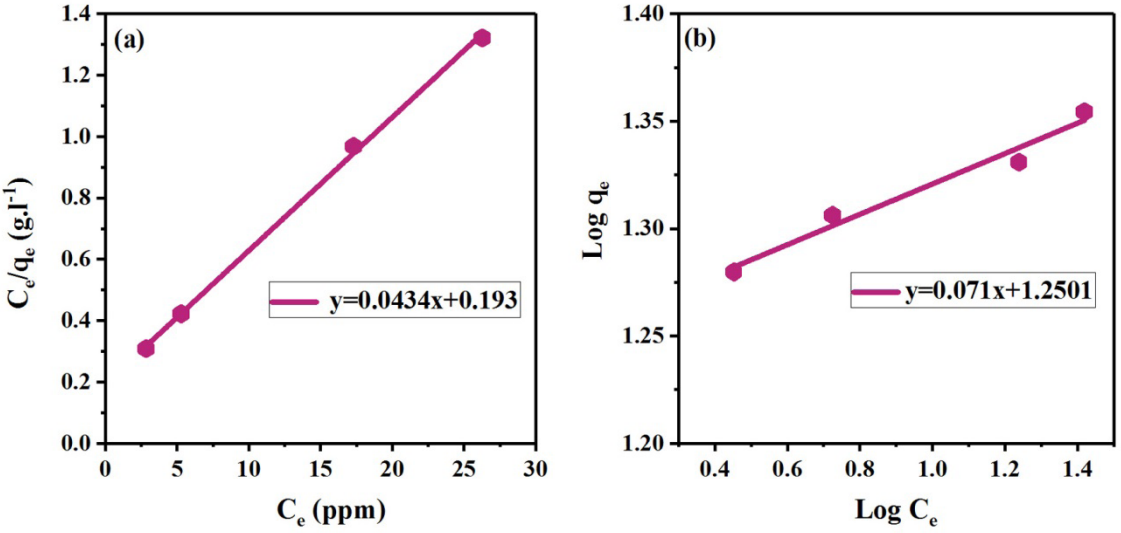

Figure 4. Absorption equilibrium assessment for $Fe_2O_3/CeO_2/Ag$ CNPs

A: Langmuir; and B: Freundlich plots for 2,4-D absorption using $Fe_2O_3/CeO_2/Ag$ sample.

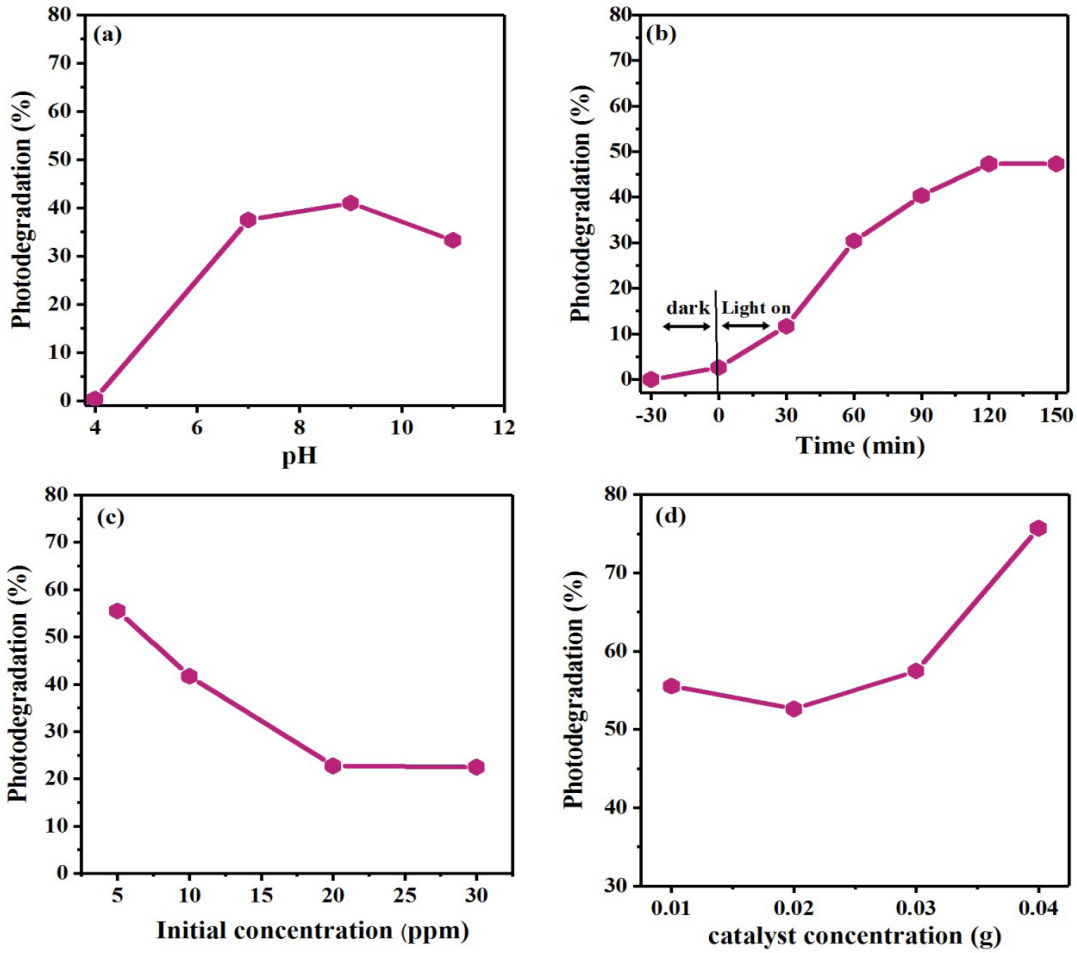

Figure 5. The experiments of performed to investigate the effects of pH, irradiation time, 2,4-D concentration, and catalyst dose on the 2,4-D photodegradation

The effect of A: pH; B: Irradiation time; C: Initial 2,4-D concentration; and D: Catalyst dose on the 2,4-D photodegradation.

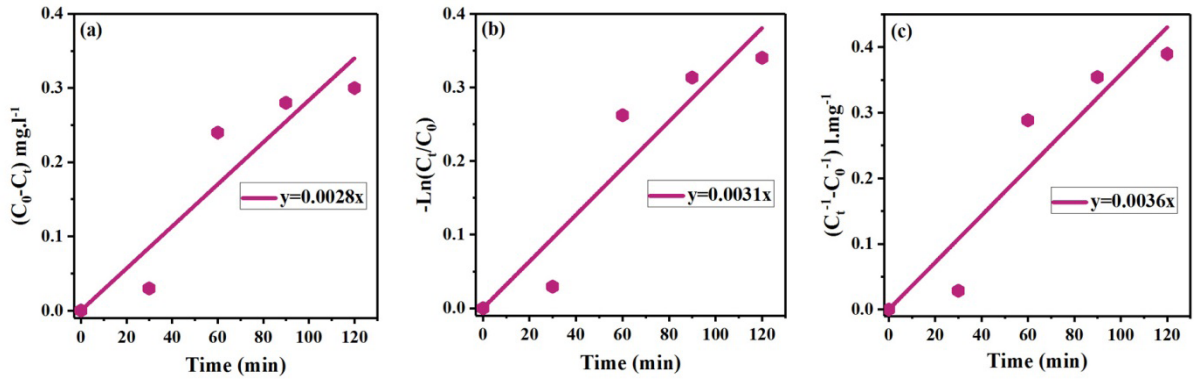

Figure 6. The reaction rate constants along with the corresponding correlation coefficients for $Fe_2O_3/CeO_2/Ag$ CNPs

A: Zero; B: First; and C: Second-order kinetic curves.

$Fe_2O_3/CeO_2/Ag$ CNPs. The effect of catalyst dose on 2,4-D photodegradation was examined in samples with pH 9, initial 2,4-D concentration of 5 ppm, and an irradiation period of 120 min. Figure 5-D illustrates the photodegradation percentage for different catalyst amounts (0.01, 0.02, 0.03, and 0.04 g). The results revealed an enhancement in photodegradation rate from about 55.55% to 75.70% with the increase of catalyst amount from 0.01 to 0.04 g, suggesting an optimal amount of 0.04 g for $Fe_2O_3/CeO_2/Ag$ CNPs.

In order to assess the reaction kinetics of photodegradation, kinetic models of Langmuir Equation were employed, as shown below, where, k0, k1 and k2 are the reaction rate constants [32]:

(6) $(C_0-C_1)=k_0t$

(7) $-h\left[\frac{C_t}{C_0}\right]=k_1t$

(8) $\left[\frac{1}{C_t}-\frac{1}{C_0}\right]=k_2t$

The experiments were performed under optimum conditions. The k values were calculated from the slop of Equations 6, 7, and 8, and the best-fitting kinetic model was estimated using the highest correlation coefficients (R^2). Table 2 and Figure 6 present the reaction rate constants along with the corresponding correlation coefficients for $Fe_2O_3/CeO_2/Ag$ CNPs. As can be seen, the photodegradation reaction of 2,4-D had the second-order reaction kinetics. The photocatalytic experiments were conducted under optimum conditions to compare the photodegradation performance of

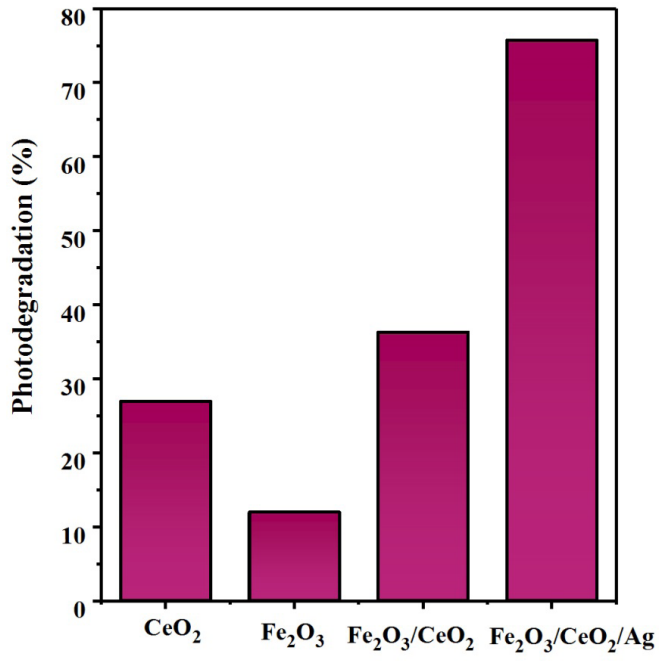

Figure 7. Comparison of 2,4-D photodegradation with CeO_2, Fe_2O_3, Fe_2O_3/CeO_2 and $Fe_2O_3/CeO_2/Ag$ CNPs

as-synthesized samples. The results for CeO_2, Fe_2O_3, Fe_2O_3/CeO_2, and Fe_2O_3/CeO_2/Ag nanostructures are illustrated in Figure 7. It can be seen that the 2,4-D photodegradation was at the highest level using Fe_2O_3/CeO_2/Ag CNPs, where the degradation rate had a trend as: Fe_2O_3/CeO_2/Ag (75.70%) >Fe_2O_3/CeO_2 (36.28%)> CeO_2 (26.92)>Fe_2O_3 (11.96).

In this study, a simple co-precipitation technique was utilized to synthesize Fe_2O_3/CeO_2/Ag CNPs. The structural characteristics were analyzed using XRD, FESEM, X-ray analysis. The photocatalytic studies were carried out to degrade 2,4-D under UV light irradiation. The conditions of the photocatalytic reaction were optimized by changing pH, irradiation time, initial 2,4-D concentration, and catalyst dose. The photocatalytic kinetic data were examined using Langmuir-Hinshelwood model, while the absorption equilibrium isotherms were studied by Langmuir and Freundlich models. Numerous studies have been conducted for the removal of 2,4-D in different conditions. In a study, it was reported that the 2,4-D degradation rate constant was highly dependent on the initial pH and temperature, in accordance with the Arrhenius model, with an apparent activation energy of 135.24 kJ/mol [33].

In another study, Fe^0@Fe_3O_4 nanoparticles with dispersibility and stability better than single nano Zero-Valent Iron (nZVI) were synthesized and combined with hydrogen peroxide to constitute a heterogeneous Fenton-like system, which was creatively applied in the degradation of 2,4-D. The effects of different reaction conditions like pH, temperature, and catalyst dosage on the removal of 2,4-D were also evaluated [34]. In another study, the characterization of Ag nanoparticles revealed that the particle size of the silver nanoparticles can be easily altered depending on the size of IL alkyl chain and anion, to produce ultrafine particles ranging 8-25 nm. Meanwhile, the photocatalytic activity of AgTf2N nanoparticles effectively degraded the highest amount of 2,4-D herbicide at 65.61%. The optimized model gave high removal percentage of 2,4-D at 97.80% (pH= 3.24; catalyst dosage= 0.009 g/L; 2,4-D concentration= 8.15 mg/L) with validation experiments of 1.28% error [35].

4. Conclusion

The highest photodegradation percentage for Fe_2O_3/CeO_2/Ag CNPs has a degradation order as Fe_2O_3/CeO_2/Ag (75.70%) >Fe_2O_3/CeO_2 (36.28%) >CeO_2 (26.92) >Fe_2O_3 (11.96).

Ethical Considerations

Compliance with ethical guidelines

There were no ethical consideration to be considered in this research.

Funding

This article was extracted from the PhD. dissertation of the first author approved by the Department of Environmental Engineering, Islamic Azad University, Ahvaz Branch.

Authors' contributions

Conceptualization and methodology: Zohreh Karimipour; Writing – original draft, and writing – review & editing: Mohammad Kazem Mohammadi; Data collection: Azadeh Haghighatzadeh and Mohammadi Rouzbahani; Data analysis and funding acquisition and resources: Reza Jalilzadeh Yengejeh.

Conflict of interest

The authors declared no conflict of interest.

Acknowledgements

This study was partially supported by Ahvaz Branch of Islamic Azad University and the authors would like to thank the Research Council for their generous support of this research.

References

[1] Brillas E, Calpe JC, Casado J. Mineralization of 2,4-D by advanced electrochemical oxidation processes. Water Res. 2000; 34(8):2253-62. [DOI:10.1016/S0043-1354(99)00396-6]

[2] Orooji N, Takdastan A, Yengejeh RJ, Jorfi S, Davami AH. Photocatalytic degradation of 2,4-dichlorophenoxyacetic acid using Fe_3O_4@ TiO_2/Cu_2O magnetic nanocomposite stabilized on granular activated carbon from aqueous solution. Res Chem Intermediates. 2020; 46(5):2833–57. [DOI:10.1007/s11164-020-04124-9]

[3] Wang Q, Wang B, Ma Y, Xing S. Enhanced superoxide radical production for ofloxacin removal via persulfate activation with Cu-Fe oxide. Chem Eng J. 2018; 354:473-80. [DOI:10.1016/j.cej.2018.08.055]

[4] Golshan M, Kakavandi B, Ahmadi M, Azizi M. Photocatalytic activation of peroxymonosulfate by TiO_2 anchored on cupper ferrite (TiO_2@ $CuFe_2O_4$) into 2,4-D degradation: Pro-

cess feasibility, mechanism and pathway. J Hazard Mater. 2018; 359:325-37. [DOI:10.1016/j.jhazmat.2018.06.069] [PMID]

[5] Chen H, Zhang Z, Feng M, Liu W, Wang W, Yang Q, et al. Degradation of 2,4-dichlorophenoxyacetic acid in water by persulfate activated with FeS (mackinawite). Chem Eng J. 2017; (313):498-507. [DOI:10.1016/j.cej.2016.12.075]

[6] Deonikar VG, Reddy KK, Chung WJ, Kim H. Facile synthesis of Ag3PO4/g-C3N4 composites in various solvent systems with tuned morphologies and their efficient photocatalytic activity for multi-dye degradation. J Photochem Photobiol: A Chem. 2019; 368: 168-81. [DOI:10.1016/j.jphotochem.2018.09.034]

[7] Kearns JP, Wellborn LS, Summers RS, Knappe DRU. 2,4-D adsorption to biochars: Effect of preparation conditions on equilibrium adsorption capacity and comparison with commercial activated carbon literature data. Water Res. 2014; 62:20-8. [DOI:10.1016/j.watres.2014.05.023] [PMID]

[8] Yang Z, Xu X, Dai M, Wang L, Shi X, Guo R. Rapid degradation of 2,4-dichlorophenoxyacetic acid facilitated by acetate under methanogenic condition. Bioresour Technol. 2017; 232:146-51. [DOI:10.1016/j.biortech.2017.01.069] [PMID]

[9] Sun C, Baig SA, Lou Z, Zhu J, Wang Z, Li X, et al. Electrocatalytic dechlorination of 2,4-dichlorophenoxyacetic acid using nanosized titanium nitride doped palladium/nickel foam electrodes in aqueous solutions. Appl Catal B. 2014; 158-159:38-47. [DOI:10.1016/j.apcatb.2014.04.004]

[10] Schenone AV, Conte LO, Botta MA, Alfano OM. Modeling and optimization of photo-Fenton degradation of 2,4-D using ferrioxalate complex and Response Surface Methodology (RSM). J Environ Manage. 2015; 155:177-83. [DOI:10.1016/j.jenvman.2015.03.028] [PMID]

[11] Cai J, Zhou M, Pan Y, Lu X. Degradation of 2,4-dichlorophenoxyacetic acid by anodic oxidation and electro-Fenton using BDD anode: Influencing factors and mechanism. Sep Purif Technol. 2020; 230:115867. [DOI:10.1016/j.seppur.2019.115867]

[12] Yang Z, Shi X, Dai M, Wang L, Xu X, Guo R. Promoting degradation of 2,4-dichlorophenoxyacetic acid with fermentative effluents from hydrogen-producing reactor. Chemosphere. 2018; 201:859-63. [DOI:10.1016/j.chemosphere.2018.03.072] [PMID]

[13] Li X, Zhou M, Pan Y. Enhanced degradation of 2,4-dichlorophenoxyacetic acid by pre-magnetization Fe-C activated persulfate: Influential factors, mechanism and degradation pathway. J Hazard Mater. 2018; 353:454-65. [DOI:10.1016/j.jhazmat.2018.04.035] [PMID]

[14] Cai J, Zhou M, Yang W, Pan Y, Lu X, Serrano KG. Degradation and mechanism of 2,4-dichlorophenoxyacetic acid (2,4-D) by thermally activated persulfate oxidation. Chemosphere. 2018; 212:784-93. [DOI:10.1016/j.chemosphere.2018.08.127] [PMID]

[15] Li W, Li Y, Zhang D, Lan Y, Guo J. CuO-Co_3O_4@ CeO_2 as a heterogeneous catalyst for efficient degradation of 2,4-dichlorophenoxyacetic acid by peroxymonosulfate. J Hazard Mater. 2020; 381:121209. [DOI:10.1016/j.jhazmat.2019.121209] [PMID]

[16] Sandeep S, Nagashree KL, Maiyalagan T, Keerthiga G. Photocatalytic degradation of 2,4-dichlorophenoxyacetic acid-A comparative study in hydrothermal TiO2 and commercial TiO_2. Appl Surf Sci. 2018; 449:371-9. [DOI:10.1016/j.apsusc.2018.02.051]

[17] Safa S, Mirzaei M, Kazemi F, Ghaneian MT, Kaboudin B. Study of visible-light photocatalytic degradation of 2,4-dichlorophenoxy acetic acid in batch and circulated-mode photoreactors. J Environ Health Sci Eng. 2019; 17(1):233-45. [DOI:10.1007/s40201-019-00343-4] [PMID] [PMCID]

[18] Tho NTM, Khanh DN, Thang NQ, Lee YI, Phuong NTK. Novel reduced graphene oxide/ZnBi2O4 hybrid photocatalyst for visible light degradation of 2,4-dichlorophenoxyacetic acid. Environ Sci Pollut Res Int. 2020; 27(10):11127-37. [DOI:10.1007/s11356-020-07752-1] [PMID]

[19] Ebrahimi R, Mohammadi M, Maleki A, Jafari A, Shahmoradi B, Rezaee R, et al. Photocatalytic degradation of 2,4-dichlorophenoxyacetic acid in aqueous solution using Mn-doped ZnO/graphene nanocomposite under LED radiation. J Inorg Organomet Polym Mater. 2020; 30(3):923-34. [DOI:10.1007/s10904-019-01280-3]

[20] Li J, Guan W, Yan X, Wu Z, Shi W. Photocatalytic ozonation of 2,4-dichlorophenoxyacetic acid using LaFeO3 photocatalyst under visible light irradiation. Catal Letters. 2018; 148:23-9. [DOI:10.1007/s10562-017-2206-2]

[21] Zhang X, Liu H, Li W, Cui G, Xu H, Han K, et al. Visible-light photocatalytic degradation of aromatic contaminants with simultaneous H2 generation: Comparison of 2,4-dichlorophenoxyacetic acid and 4-chlorophenol. Catal Letters. 2008; 125:371-5. [DOI:10.1007/s10562-008-9542-1]

[22] Chawla S, Uppal H, Yadav M, Bahadur N, Singh N. Zinc peroxide nanomaterial as an adsorbent for removal of Congo red dye from waste water. Ecotoxicol Environ Saf. 2017; 135:68-74. [DOI:10.1016/j.ecoenv.2016.09.017] [PMID]

[23] Gashtasbi F, Yengejeh RJ, Babaei AA. Photocatalysis assisted by activated-carbon-impregnated magnetite composite for removal of cephalexin from aqueous solution. Korean J Chem Eng. 2018; 35(1):1726-34. [DOI:10.1007/s11814-018-0061-5]

[24] Gashtasbi F, Yengejeh RJ, Babaei AA. Adsorption of vancomycin antibiotic from aqueous solution using an activated carbon impregnated magnetite composite. Desalination Water Treat. 2017; 88:286-97. [DOI:10.5004/dwt.2017.21455]

[25] Yoon KH, Noh JS, Kwon CH, Muhammed M. Photocatalytic behavior of TiO2 thin films prepared by sol-gel process. Mater Chem Phys. 2006; 95(1):79-83. [DOI:10.1016/j.matchemphys.2005.06.001]

[26] Zhang L, Li H, Liu Y, Tian Z, Yang B, Sun Z, et al. Adsorption-photocatalytic degradation of methyl orange over a facile one-step hydrothermally synthesized TiO2/ZnO-NH2-RGO nanocomposite. RSC Adv. 2014; 4(89):48703-11. [DOI:10.1039/C4RA09227A]

[27] Mekatel E, Amorkrane S, Trari M, Nibou D, Dahdouh N, Ladjali S. Combined adsorption/photocatalysis process for the decolorization of acid orange 61. Arabian J Sci Eng. 2019; 44:5311-22. [DOI:10.1007/s13369-018-3575-6]

[28] El-Moselhy MM, Kamal SM. Selective removal and preconcentration of methylene blue from polluted water using cation exchange polymeric material. Groundw Sustain Dev. 2018; 6:6-13. [DOI:10.1016/j.gsd.2017.10.001]

[29] Nekouei F, Nekouei S. Comparative evaluation of BiOCl-NPls-AC composite performance for methylene blue dye removal from solution in the presence/absence of UV irradiation: Kinetic and isotherm studies. J Alloys Compd. 2017; 701:950-66. [DOI:10.1016/j.jallcom.2017.01.157]

[30] Ali A, Mannan A, Hussain I, Hussain I, Zia M. Effective removal of metal ions from aquous solution by silver and zinc nanoparticles functionalized cellulose: Isotherm, kinetics and statistical supposition of process. Environ Nanotechnol Monit Manag. 2018; 9:1-11. [DOI:10.1016/j.enmm.2017.11.003]

[31] Gunasundari E, Senthil Kumar P. Adsorption isotherm, kinetics and thermodynamic analysis of Cu (II) ions onto the dried algal biomass (Spirulina platensis). J Ind Eng Chem. 2017; 56:129-44. [DOI:10.1016/j.jiec.2017.07.005]

[32] Sivakumar P, Gaurav Kumar GK, Renganathan S. Synthesis and characterization of ZnS-Ag nanoballs and its application in photocatalytic dye degradation under visible light. J Nanostructure Chem. 2014; 4:107. [DOI:10.1007/s40097-014-0107-0]

[33] Cai J, Zhou M, Yang W, Pan Y, Lu X, Serrano KG. Degradation and mechanism of 2,4-dichlorophenoxyacetic acid (2,4-D) by thermally activated persulfate oxidation. Chemosphere. 2018; 212:784-93. [DOI:10.1016/j.chemosphere.2018.08.127] [PMID]

[34] Lv X, Ma Y, Li Y, Yang Q. Heterogeneous fenton-like catalytic degradation of 2,4-dichlorophenoxyacetic acid by nanoscale zero-valent iron assembled on magnetite nanoparticles. Water. 2020; 12(10):2909. [DOI:10.3390/w12102909]

[35] Kamarudin NS, Jusoh R, Jalil AA, Setiabudi HD, Sukor NF. Synthesis of silver nanoparticles in green binary solvent for degradation of 2,4-D herbicide: Optimization and kinetic studies. Chem Eng Res Des. 2020; 159:300-14. [DOI:10.1016/j.cherd.2020.03.025]